Science of the Total Environment 751 (2021) 141491

Contents lists available at ScienceDirect

Science of the Total Environment

journal homepage: www.elsevier.com/locate/scitotenv

Effects of feedstock biopolymer compositions on the physiochemical characteristics of dissolved black carbon from lignocellulose-based biochar

Lu Han [a,d], Xiang Nie [a,d], Jing Wei [b], Mingyue Gu [c], Wenpei Wu [a,d], Mengfang Chen [a,d,*]

[a] Key Laboratory of Soil Environment and Pollution Remediation, Institute of Soil Science, Chinese Academy of Sciences, Nanjing 210008, China
[b] Key Laboratory of Coastal Environmental Processes and Ecological Remediation, Yantai Institute of Coastal Zone Research, Chinese Academy of Sciences, Yantai 264003, China
[c] Nanjing Kaiye Environmental Technology Co Ltd, 8 Yuanhua Road, Innovation Building 106, Nanjing University Science Park, Nanjing 210034, China
[d] Jiangsu Engineering Laboratory for Soil and Groundwater Remediation of Contaminated Sites, Institute of Soil Science, Chinese Academy of Sciences, Nanjing 210008, China

HIGHLIGHTS

- DBC formation was associated with different biopolymer compositions with HTT varying.
- The pyrolysis of CEL and HEM had significant effects on DBC properties under low HTT.
- DBC properties were closely related to LIG and its proportions in biomass under high HTT.
- LIG-rich DBCs illustrated more surface negative charges and transport potential.

GRAPHICAL ABSTRACT

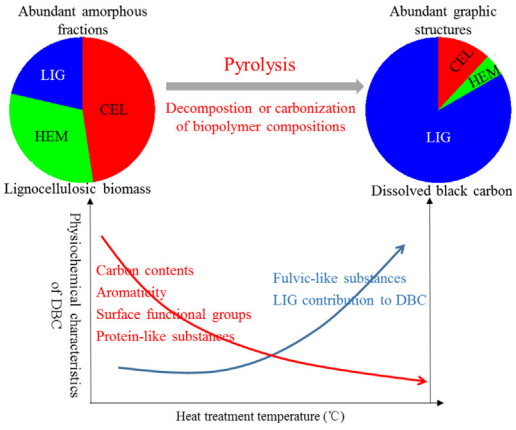

ARTICLE INFO

Article history:
Received 17 May 2020
Received in revised form 30 July 2020
Accepted 3 August 2020
Available online 4 August 2020

Editor: Baoliang Chen

Keywords:
Biochar
Dissolved black carbon
Biopolymer compositions
Lignocellulose

ABSTRACT

Dissolved black carbon (DBC) is becoming increasingly concerned by researchers due to its unique environmental behavior. However, understanding of the influence mechanism of biopolymer compositions of cellulose (CEL), hemicellulose (HEM) and lignin (LIG) on the formation and physiochemical characteristics of DBC from lignocellulose-based biochar is limited. This study therefore examined the formation of DBCs derived from the biopolymer compositions, corn straw (CS), corncob (CC), bamboo sawdust (BS) and pinewood sawdust (PS) under the heat treatment temperatures (HTTs) of 300–500 °C. Zeta potential and hydrodynamic diameters (D_h) of DBCs produced under 300 °C were further investigated. DBC formation may be closely associated with the HTT-dependent heterogeneities of biopolymer compositions, in which significant effects of CEL and HEM charring on physiochemical properties of DBCs were identified under the HTT of 300 and 400 °C, while the formation of DBCs was closely related to LIG and its proportions in biomass under high HTT (>500 °C). On the rise of the HTT, the carbonaceous structures of biopolymer compositions were reorganized and converted to graphitic structures in biochar accompanied by the large decomposition or carbonization of CEL and HEM, leading to the reduced carbon content, surface functional groups, aromaticity and molecular weight of DBCs, as well as the decrease of protein-like and relative increase of fulvic-like fluorescent substances in most DBCs. LIG in biomass

* Corresponding author at: Key Laboratory of Soil Environment and Pollution Remediation, Institute of Soil Science, Chinese Academy of Sciences, Nanjing 210008, China.
E-mail address: mfchen@issas.ac.cn (M. Chen).

https://doi.org/10.1016/j.scitotenv.2020.141491

may facilitate the migration of DBCs due to abundant surface negative charges and the formation of low D_h. This study offered new insights into our understanding of influencing mechanisms of biopolymer compositions on the characteristic of DBCs under different HTTs.

1. Introduction

Biochar, derived from the pyrolysis of biomass, has gained worldwide attention for its potential application for agronomic and environmental benefits (Qu et al., 2016; Han et al., 2017; Ouyang et al., 2017). In addition, Biochar was reported to amend the trace metal bioavailability, soil microbial activity and soil dissolved organic matter (DOM) (Yang et al., 2019). Lignocellulosic biomass, including cellulose (CEL), hemicellulose (HEM) and lignin (LIG) as the main structural biopolymers, is the most abundant, green and renewable sources worldwide (Zhao et al., 2014). There is approximately 1.98×10^8 tons of corncob alone generated annually in the world (Shao et al., 2020) and a large amount of the agricultural waste was not well utilized. The pyrolysis of lignocellulosic biomass to produce biochar is a vital thermo-chemical conversion method for effective utilization of lignocellulosic biomass, such as agricultural and plant waste (Biswas et al., 2018; Gai et al., 2013). In comparison with bulk biochar, the water-extractable substance from biochar, termed as dissolved organic matter or dissolved black carbon (DBC), generally being separated by filtrating through the 0.45-μm filter membrane, could be readily released into the environment (Qu et al., 2016). DBC could influence many geological and environmental processes, and readily migrate in subsurface and further regulate the fate and transport of contaminants such as inorganic, organic, and pathogenic microorganism (Chen et al., 2017; Huang et al., 2019). DBC is reported to interact with heavy metals (Chen et al., 2015), alter the surface charge of particles, adsorb to mineral surfaces, intervene in mineral dissolution/precipitation reactions, and drive redox and photochemical reactions (Aiken et al., 2011). DOM also plays significant roles in changing the toxicity and heavy metals in soils (Soja et al., 2018). Initial investigations have stated that DBC could facilitate the migration of natural solutes and contaminants, such as increasing the leaching of phosphorus in alkaline soil (Chen et al., 2018) and enhancing desorption and mobility of arsenic in soil and groundwater (Kim et al., 2018; Zhong et al., 2020). The biochar colloid less than 1 μm was also proved to adsorb and carry more heavy metals than bulk biochar (Qian et al., 2016). In addition, DBC is also reported to exhibit adverse effect on the ecosystem, for instance, the DBC derived from LIG-rich pinewood biochar is more toxic to the aquatic photosynthetic microorganisms than that derived from CEL-rich peanut shell biochar (Smith et al., 2013). In addition, compared with DBCs derived from sludge and rice biochar, it would be easy for the corn biochar-derived DBC to form the carcinogenic disinfection byproducts such as trihalomethanes and haloacetic acids (Lee et al., 2018). Clearly, the properties of DBC, regulating their environmental impact, are determined by the compositions and structure-specific pyrolysis (Liu et al., 2018). However, current understanding on the relationship of the structures and compositions of feedstock with their pyrolysis processes and consequently the properties of the obtained DBC is rather limited. A detailed investigation on biomass pyrolysis in relation to the physicochemical properties of DBC is urgently needed. This line of study will also greatly facilitate in understanding undesirable effects of DBC on the environment and regulating their properties to suit specific applications.

It is generally agreed that the characteristics of DBC derived from lignocellulose-based biochar are closely associated with the nature of feedstock and heating temperatures (Liu et al., 2015; Tripathi et al., 2016). Clear differences in the properties of DBC in biochar made from the same feedstock under different pyrolytic conditions have been observed (Jamieson et al., 2014). Numerous studies have investigated the properties of DBCs originated from some lignocellulosic biomass biochar (Lin et al., 2012; Norwood et al., 2013; Li et al., 2017; Song et al., 2019). It is identified that the contents of DBCs released from herbaceous-biochar were higher than those from woody plants-biochar, which were markedly decreased with the increase of pyrolytic temperatures for both types of biochar (Qu et al., 2016; Song et al., 2019) and were progressively decreased following the increase of the heat treatment temperature (HTT) accompanied by an increase in thermally stable graphic carbon fractions (Uchimiya et al., 2013). Compared with bulk biochar, DBC contained more oxygen and polar functional groups and fewer aromatic structures, leading to lower carbon stability, but better dispersibility in water (Lian and Xing, 2017). Smith et al. (2013) also reported that DBC derived from pinewood biochar showed unique carbohydrate ligneous and sulfur containing condensed ligneous components, which are both absent from the DBC derived from peanut shell biochar. However, physicochemical characteristics of DBC, such as chemical structure and surface charge, were reported without discussing the influencing mechanism of biopolymer compositions and HTT on the DBC formation (Song et al., 2019; Lian and Xing, 2017).

Therefore, the main objective of this study is to compare the physicochemical characteristics of DBCs derived from four lignocellulosic biomass and three biopolymer compositions under different HTTs. CEL- and HEM-rich biomass such as corn straw and corncob, and LIG-rich biomass such as bamboo sawdust and pinewood sawdust are selected as the feedstock because they are widely distributed agriculture and woody plant residues in Asian countries (Wang et al., 2013; Li et al., 2014). Multiple analysis methods including DOC determination, UV–vis spectroscopy, fluorescence spectroscopy and parallel factor analysis, fourier transform infrared spectroscopy and zeta potential analysis will be combined. Specifically, revealing the physicochemical characteristics of DBC derived from biochar may provide new insights into our understanding of influencing mechanisms of biopolymer compositions on the characteristics of DBCs under different HTTs.

2. Materials and methods

2.1. Preparation of biochar

Commercial CEL, HEM, LIG, bamboo sawdust (BS) and pinewood sawdust (PS) were purchased from Bomei biological Co., Ltd. (Hefei, China). Corn straw (CS) and corncob (CC) were collected from the local farmland of Nanjing, Jiangsu Province, China. The content of CEL, HEM and LIG component in the four biomasses is listed in Table S1 in Supporting Information (SI). Their LIG content is increased in turn as 9%, 14%, 21% and 28% in CS, CC, BS and PS (Zhong et al., 2011; Yang et al., 2005; Ando et al., 2000; He et al., 2019).

The clean biomass (<0.154 mm) was carbonized under three HTTs (i.e. 300, 400 and 500 °C) respectively for 3 h with the programmed incremental temperature rate of 5 °C/min. The obtained biochar were grounded to pass through a 0.154-mm sieve and kept in the brown glass bottles. The biochar derived from HEM prepared at 500 °C was completely consumed due to the heat expands of HEM as observed in our previous study (Han et al., 2016). Therefore, twenty biochar were ultimately obtained.

2.2. Extraction of DBC

The water-extracted DBC was obtained by soaking 5.0 g as-obtained biochar sample in 500 mL of ultrapure water and agitating on a

reciprocating shaker at 150 rpm at 25 °C for 72 h. Two replicates for each type of biochar and an ultrapure water-only control were designed. Consequently, the suspensions passing through a 0.45-μm nylon membrane was defined as DBC which was abbreviated as a precursor followed by the HTT, i.e. DCS300 representing DBC derived from corn straw under the HTT of 300 °C. The pH of DBC suspensions was measured and ranged from 6.97 to 8.02, 7.76 to 10.11, 7.46 to 10.27, 7.28 to 8.58, 5.08 to 7.26, 4.07 to 6.71, 10.72 to 11.50, respectively for those derived from BS, CC, CS, PS, CEL, HEM and LIG biochar under HTTs from 300 to 500 °C (Fig. S1). Duplicates of DBC samples (10 mL) were collected to determine the concentration of dissolved organic carbon (DOC) using a TOC-L analyzer equipped with an ASI-L auto sampler (Shimadzu, Japan). The DBC contents (mg C/g biochar) were calculated as the volume of extraction water (L) multiplied by the DOC concentration (mg/L) and divided by the mass of biochar (g). The cations including K^+, Ca^{2+}, Na^+, Mg^{2+}were measured using a PerkinElmer Avio 200-ICP-OES (Hitachi, Japan) and anions were using a Dionex™ ICS-5000$^+$ DP ion chromatograph (Thermo Fisher Scientific, USA) for Cl^-, Br^- and SO_4^{2-} determination and a SAN++ continuous flowing analyzer (SKALAR, Netherlands) for $NO_3^- + NO_2^-$ determination in the DBC suspensions. Consequently, the remaining liquid samples were freeze-dried to obtain the DBCs as dry solids and stored in a desiccator in the dark until use.

2.3. Characterization of DBC

UV–vis spectroscopy under the specific ultraviolet absorbance wavelength of 200–600 nm was obtained using a UV-6700 UV–visible spectrophotometer (Shimadzu, Japan). The spectral absorption ratio of 254 to 365 nm (E_2/E_3 ratio) and spectral slopes for the intervals of 275–295 nm ($S_{275–295}$) were determined to reflect the aromaticity and mean molecular weight (M_w) (Liu et al., 2019). The detailed calculation method was given in SI.

For ATR-FTIR analysis, the freezing dried DBC samples were mixed with potassium bromide at a ratio of 1:200 and performed on a Thermo Nicolet iS10 FTIR. The scanning region ranges from 400 cm^{-1} to 4000 cm^{-1} and the standard parameter for data collection was set at 64 scans with 1.0 cm^{-1} resolution.

Fluorescence excitation-emission (EEM) spectra were obtained using an Aqualog spectrofluorometer (HORIBA, Japan). The emission wavelength (Em) range was set from 250 to 600 nm in steps of 1 nm, and the excitation wavelength (Ex) range was set from 200 to 450 nm in steps of 5 nm. Ultrapure water-only control was measured and the EEMs were subtracted from the DBC measurements to remove Raman scattering effects. Fluorescence indices, such as fluorescence index (FI), biological index (BIX) and humification index (HIX) were used to characterize the optical properties of DBC. FI provides information on the sources (e.g., microbial or terrestrial plant material) or degrees of degradation of DOM; HIX is an indicator of humic substances or extent of humification (Fellman et al., 2010); BIX typically reflects microorganisms' activities, and is related to increasing algal- or/and bacteria-derived particulate organic matter (Yang et al., 2014). Details of the calculated method were given in SI. The approach of PARAFAC modeling was used to resolve the dominant fluorescent DOM components based on their excitation and emission (Ex/Em) maxima (Ishii and Boyer, 2012; Wei et al., 2019).

Distributions of the hydrodynamic diameters (D_h) and zeta potentials of DBC were measured by dynamic light scattering (DLS) using a Zetasizer Nano ZS90 analyzer (Malvern, U.K.) with a fixed scattering angle of 90° at 25 °C. The DBC suspension with DOC concentration of 10 mg/L under the solution pH ranging from 1.50 to 6.00 was sonicated for 30 min before D_h and zeta potentials determination. Five replicates with more than 20 runs per measurement were conducted for each sample (Wang et al., 2019).

2.4. Statistical analysis

All statistical analyses were carried out using SPSS V.18 for Windows (IBM Corporation, USA). The average value and standard deviation of the experiment data were calculated. Bivariate correlation analysis of data was carried out.

3. Results and discussions

3.1. DBC formation

As illustrated in Fig. 1, the mean DOC concentrations of DBCs released from the selected biochar were in the increased order of DCC300 (7.69 ± 1.65 mg/L) < DCEL300 (9.65 ± 2.36 mg/L) < DBS300 (13.69 ± 2.61 mg/L) < DHEM300 (21.01 ± 4.20 mg/L) < DPS300 (29.82 ± 1.41 mg/L) < DCS300 (48.98 ± 2.63 mg/L) < DLIG300 (971.81 ± 38.20 mg/L). The contents of DBCs derived from biochar in the present study and previously published data are summarized in Table S2. It is observed that a great variation in the contents of DBCs derived from different biochar ranged from 0.045 to 97.18 mg C/g. These may have been caused by the differences among feedstock types, pyrolytic conditions and extraction protocols (Qu et al., 2016). However, it is identified that the contents of DBCs derived from CEL- and HEM-rich biochar were mostly higher than those from LIG-rich biochar (Smith et al., 2013; Jamieson et al., 2014; Qu et al., 2016; Liu et al., 2018) except for DCC300 with relative low DOC concentration in this experiment. Liu et al. (2018) found that the content of nano biochar derived from furfural residues was much lower than those from peanut shell, cotton straw and Chinese medicine residues, due to higher content of lignin (45.2% vs 12.1–23.4%) and lower cellulose (22.1% vs 38.9–48.2%) in furfural residues compared with those in other feedstock. This is because abundant graphitic structures from carbonizing LIG make it difficult to release nano biochar (Liu et al., 2018). It is also proved that few nano biochar were released from coal and natural graphite activated carbons but more nano biochar were observed from coconut husk activated carbon that contains abundant amorphous fractions (Liu et al., 2018). Consequently, it is speculated that the disordered, loose and amorphous fractions such as CEL and HEM in biochar are prone to be converted to DBCs under low HTT. In addition, the experimental results showed that HEM was more readily degraded into DBCs than CEL under the HTT of 300 °C, and this is supported by the DOC concentration of 21.01 ± 4.20 mg/L for DHEM300 being greater than 9.65 ± 2.36 mg/L for DCEL300. This is ascribed to the abundant random and amorphous structure with many branches in HEM (Han et al., 2016). In addition, it is inferred that some other reasons may be responsible for the less content of DBCs derived from corncob biochar. Firstly, the ash contents of corncob biochar ranged from 1.59% to 2.92%, which are close to those of pinewood sawdust biochar (1.02%–3.63%) but much lower than those of corn straw

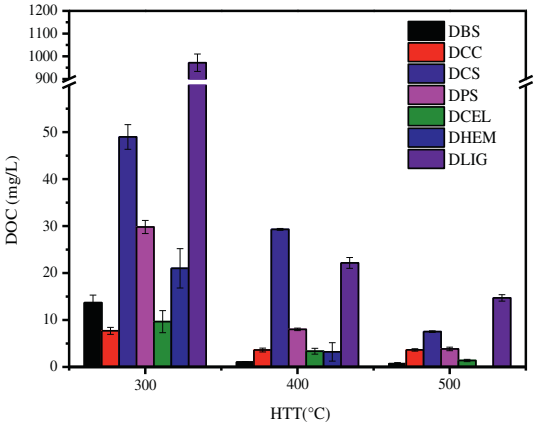

Fig. 1. DOC concentrations of dissolved black carbons (DBCs) derived from biochar under different heat treatment temperatures (HTTs). Note: DBS, DCC, DCS, DPS, DCEL, DHEM and DLIG represents DBC derived from bamboo sawdust, corncob, corn straw, pinewood sawdust, cellulose, hemicellulose and lignin biochar, respectively.

biochar (9.70%–16.20%) as shown in Fig. S2, potentially leading to the small release of DBC from corncob biochar since the presence of inorganic species could promote the release of DBC (Smith et al., 2013; Zhao et al., 2016; Song et al., 2019). Secondly, the structure of biopolymer compositions in corncob was more rigid than that in corn straw, which may make it difficult to form DBC. Overall the reason for low release of DBC derived from corncob biochar warrants further investigation.

However, it should be noted that the content of DLIG300 is substantially higher than other DBCs contents. This is in contradiction with the conclusion mentioned above. LIG is a complex and non-crystalline three-dimensional network of phenolic polymers with phenyl propane as the main structure and cross-linked with CEL and HEM through covalent bonds and hydrogen bonds (Cao et al., 2018). The commercial production of LIG is originated from black liquor, a waste product of the alkaline Kraft process in wood pulping (Fan et al., 2017). It is speculated that the alkaline suspensions of LIG biochar with pH ranging from 10.72 to 11.50 (Fig. S1) was favorable for the release of DBC (Li et al., 2017). In addition, the inorganic species in LIG may also promote the release of DBC as our previous study has determined that the commercial LIG contained higher ash content at 11.07% than 0.02% and 0.01% for CEL and HEM respectively (Han et al., 2016). Therefore, this may lead to higher content of DBC derived from LIG than those from CEL and HEM.

On the rise of HTT, the DOC concentrations of DBCs were significantly declined. Still much lower DOC concentrations of DHEM400 (3.21 ± 1.96 mg/L), DCEL400 (3.56 ± 0.62 mg/L) and DCEL500 (1.37 ± 0.24 mg/L) than those of DLIG400 (22.15 ± 1.15 mg/L) and DLIG500 (14.71 ± 0.69 mg/L) indicated that most pyrolysis products of CEL and HEM may be volatiles when producing biochar following the increase of HTT. This is also supported by the result of thermogravimetric analysis that the fraction of residue weights was LIG (33.0%) > HEM (9.05%) > CEL (0.44%) in the whole pyrolysis (Tao et al., 2020). Therefore, the obtained DBC was most likely to be composed by the pyrolysis products of LIG, especially at high temperatures. The DOC concentration of 29.3 ± 0.26 mg/L for DCS400 was also much higher than 8.02 ± 0.61 mg/L and 1.03 mg/L for DPS400 and DBS400 respectively, while the differences among DCS500 (7.52 ± 0.18 mg/L), DPS500 (3.84 ± 0.37 mg/L) and DBS500 (0.69 ± 0.12 mg/L) were narrowed. It is ascribed to the reconfiguration of carbonaceous structures, leading to ordered, denser, and rigid graphitic structures formed during the pyrolysis with the increase of HTT and they were less readily degraded into DBCs (Liu et al., 2018). Another possible reason may be related to the abundant loss of HEM following the increase of HTTs and complete consumption of HEM was observed under the HTT of 500 °C, leading to the decrease on the DOC concentrations of DBCs. In addition, the concentrations of K^+, Ca^{2+}, Na^+, Mg^{2+}, Cl^-, SO_4^{2-}, Br^-, NO_3^- and NO_2^- co-released into water from biochar are provided in Table S3. The cations were significantly decreased with the increase of HTT due to the pyrolytic lost and Mg^{2+} concentration ranging from 19.04 to 431.47 mg/L were relative high in DBC derived from biomass under the HTT of 300 °C. The concentrations of Cl^- ranging from 0.38 to 50.50 mg/L and SO_4^{2-} ranging from 3.16 to 8.61 mg/L were much higher than those of Br^-, NO_3^- and NO_2^- derived from four biomasses, while Cl^- and SO_4^{2-} concentrations for DBC derived from LIG were more than 1000 mg/L. However, no significant correlation was identified between the concentrations of cations or anions and DOC with bivariate correlation analysis. Therefore, on the increase of HTT, CEL and HEM as main amorphous components was incrementally lost or converted to graphitic crystallites in biochar (Kercher and Nagle, 2003), while LIG was the least thermally stable among the three components (Yang et al., 2007; Li et al., 2014), implying that LIG may be important for the formation of DBC under high HTTs (>500 °C).

3.2. UV–vis analysis

The intensities of UV–Vis absorbance bands for the tested DBCs were all decreased with the increase of wavelengths (Fig. S3), similar to those observed for other DBCs and humic-like substances (Chen et al., 2002; Qu et al., 2016). The E_2/E_3 ratios and $S_{275-295}$ values of DBCs are presented in Fig. 2 and Table S4. Under the HTT of 300 °C, the E_2/E_3 ratios were 10.71 ± 0.12, 7.84 ± 0.90, and 3.32 ± 0.06 for DHEM300, DCEL300, and DLIG300, respectively, indicating the highest aromaticity and M_w of DLIG300 since the E_2/E_3 ratio is inversely proportional to the two characteristic parameters of DBC (Liu et al., 2019). The E_2/E_3 ratios of DCS300, DCC300, DBS300 and DPS300 ranged from 5.54 ± 0.23 to 6.44 ± 0.15, which were comparable with 4.70–7.00 for DBCs derived from wood and herbaceous residues biochar (Liu et al., 2019). This implies that the aromaticity and M_w of DBCs were possibly associated with three biopolymer compositions under the low HTTs. As the HTT was increased, the E_2/E_3 ratios of DBCs derived from CEL and HEM were markedly declined to 1.72 ± 0.14 and 6.47 ± 0.16 for DCEL500 and DHEM400 respectively, suggesting that some amorphous fractions in CEL and HEM were converted to aromatic fractions. However, the E_2/E_3 ratios of DBC derived from CS, CC, BS, PS and LIG were incrementally increased to 8.03 ± 0.53, 7.49 ± 0.05, 8.11 ± 0.36 and 8.36 ± 0.18 for DCS500, DCC500, DBS500 and DPS500 respectively, similar to 9.96 ± 0.09 for DLIG500. This finding indicated that the characteristics of aromaticity and M_w were more consistent with that of LIG accompanied by the carbonization and decomposition of CEL and HEM under 500 °C.

Variations in M_w of the DBCs could qualitatively reflected by $S_{275-295}$ values under different HTTs (Fig. 2b). A decrease in $S_{275-295}$ values

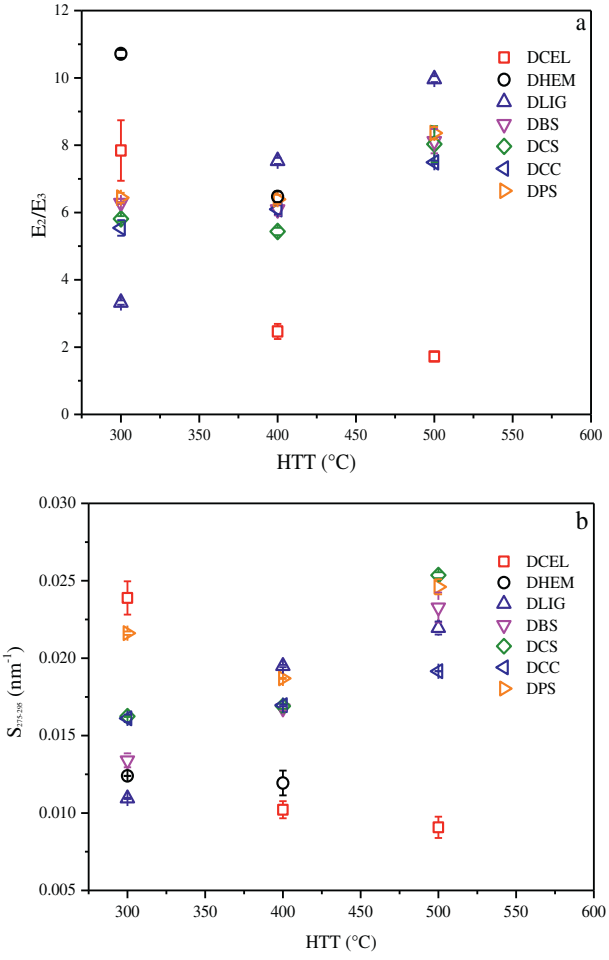

Fig. 2. UV–vis spectroscopic analyses of DBCs derived from biochar: (a) E_2/E_3 ratio and (b) $S_{275-295}$ measurements. Note: DBS, DCC, DCS, DPS, DCEL, DHEM and DLIG represents DBCs derived from bamboo sawdust, corncob, corn straw, pinewood sawdust lignin, cellulose and hemicellulose biochar, respectively.

suggests an increase in M_w (Liu et al., 2019). $S_{275-295}$ values of DBS300, DPS300, DCS300 and DCC300 ranging from 0.016 to 0.023 nm^{-1} were between 0.012 nm^{-1} for DLIG300 and 0.024 nm^{-1} for DCEL300. the M_w of DBCs were generally decreased with the HTT increasing, supported by both the increasing E_2/E_3 ratios and $S_{275-295}$ values, which was consistent with other published results (Jamieson et al., 2014). However, $S_{275-295}$ value of DBC derived from CEL was gradually decreased to 0.0091 nm^{-1} for DCEL500, similar to 0.0108 and 0.0130 nm^{-1} for DBCs derived from switch grass and soybean biochar respectively (Liu et al., 2019). Consequently, $S_{275-295}$ values of DCC500, DCS500, DPS500 and DBS500 range from 0.019 to 0.025 nm^{-1}, close to 0.022 nm^{-1} for DLIG500. Therefore, the M_w of DBCs was particularly influenced by LIG under the HTT of 500 °C.

3.3. Fluorescence spectrum analysis

3.3.1. Fluorescence EEM of DBCs

Main Ex/Em peak positions were located around 250/450 in the EEM spectra of DBCs except those derived from HEM biochar (Fig. S4). The intensities of EEM spectra of DBCs derived from LIG, CS, CC, PS and BS were increased as a function of HTT, whereas those from CEL and HEM were markedly diminished. This may be attributed to readily fluoresced aromatic, rigid compounds with low energy p-p* transition, and seldom fluoresced aliphatic compounds, because of a rapid energy transfer through overlapping vibrational levels (Uchimiya et al., 2013). The fluorescence indices including FI, HIX and BIX are shown in Table 1. The HIX values of DBCs were generally increased on the rise of HTT, indicating enhanced degree of humification similar to the published results (Fellman et al., 2010). It is notable that the HIX value of 216.25 ± 0.38 for DHEM300 is much higher than 3.85 ± 1.08 and 2.31 ± 0.23 for DLIG300 and DCEL300 respectively. The HIX values for DBS300 and DPS300 were much lower than those for DCS300 and DCC300 and the mean HIX value of the four DBCs was 1.79 ± 0.58, close to those of DLIG300 and DCEL300. As the HTT was increased, the HIX value for DCEL400 was increased to 4.78 ± 0.56 and then decreased to 3.47 ± 0.43 for DCEL500, while that of DHEM400 had sharply dropped to 14.70 ± 1.57. In comparison, the HIX value of DBC derived from LIG was continually increased with the highest value of 22.92 ± 1.04 obtained for DLIG500, indicating significantly enhanced humification similar to that of the sediment organic matter (He et al., 2016). In addition, the HIX values of DCS500, DCC500, DBS500 and DPS500 ranging from 4.71 ± 0.97 to 9.74 ± 0.73 may be integratedly influenced by LIG and CEL. However, the decomposition of CEL has been so substantial under the HTT of 500 °C that its effect on the humification was relatively weak. The FI values from the most DBCs range from 1.08 ± 0.05 to 2.05 ± 0.07, except those of DPS300 and DCEL400 reaching 3.18 ± 0.12 and 3.04 ± 0.12 respectively. In addition, the BIX values of DBCs were low ranging from 0.22 ± 0.037 to 0.99 ± 0.025 in consistency with the published results from lignoncellulose biochar (Lee et al., 2018).

Table 1
Fluorescence spectroscopic indices of DBCs derived from biochar.

DBCs	Mean HIX	SD	Mean FI	SD	Mean BIX	SD
DCS300	4.43	1.07	1.69	0.11	0.80	0.010
DCC300	2.23	1.12	1.62	0.12	0.46	0.023
DBS300	0.20	0.07	2.05	0.07	0.62	0.017
DPS300	0.30	0.06	3.18	0.12	0.53	0.012
DLIG300	3.85	1.08	1.27	0.08	0.90	0.039
DCEL300	2.31	0.23	1.64	0.11	0.44	0.032
DHEM300	216.25	0.38	1.43	0.13	0.13	0.014
DCS400	7.78	1.01	1.71	0.09	0.69	0.027
DCC400	10.71	1.37	1.43	0.07	0.47	0.033
DBS400	6.88	1.33	1.39	0.13	0.23	0.022
DPS400	8.35	1.16	1.68	0.06	0.47	0.059
DLIG400	15.17	1.27	1.54	0.11	0.73	0.061
DCEL400	4.78	0.56	3.04	0.12	0.90	0.038
DHEM400	14.70	1.57	1.08	0.05	0.12	0.037
DCS500	7.55	1.19	1.92	0.08	0.68	0.034
DCC500	6.87	1.02	1.66	0.12	0.99	0.025
DBS500	4.71	0.97	1.41	0.09	0.22	0.038
DPS500	9.74	0.73	1.55	0.12	0.48	0.026
DLIG500	22.92	1.04	1.54	0.04	0.81	0.021
DCEL500	3.47	0.43	1.24	0.10	0.51	0.018

Note: DBS, DCC, DCS, DPS, DCEL, DHEM and DLIG represents DBCs derived from bamboo sawdust, corncob, corn straw, pinewood sawdust lignin, cellulose and hemicellulose biochar, respectively. The number followed the abbreviated letters represents the heat treatment temperature. FI, fluorescence index. HIX, humification index. BIX, biological index. SD, standard deviation.

3.3.2. EEM-PARAFAC of DBCs

UVC/UVA Humic-like (C1, C2), microbial decomposition products (C3), fulvic-like (C4) and protein-like (C5) components were classified using EEM-PARAFAC analyses as shown in Fig. 3 and Table S5. C1 and C2 with the characteristic peaks at Ex/Em of 275/450 nm and <225 (305)/422 nm, respectively, can be assigned to UVC/UVA humic-like large molecular, hydrophobic (macro) molecules (Uchimiya et al., 2013; Li et al., 2017). C1 with relatively long Em had larger molecular size than C2 (Uchimiya et al., 2013) and was related to the presence of low molecular weight (poly) phenolic molecules (Uchimiya et al., 2013) and highly unsaturated aliphatic compounds (Kellerman et al., 2015). Humic substance is historically considered to have a large, high molecular weight macromolecule, however, the subsequent research suggested that aggregates of low molecular weight compounds contribute to the soil organic carbon fractions are defined as humic substance (Schmidt et al., 2011). C3 with its maximum Ex/Em peak of 270/394 nm could be assigned to microbial decomposition products of humic-like precursors and represented more soluble and labile carbon fraction having lower aromaticity than humic-like fractions (Uchimiya et al., 2013). Component C4 showing the characteristic peak at Ex/Em of 240/374 nm, was comparable to fulvic-like fluorophores including (poly)phenolic pyrolysis products (Deenik et al., 2010), which represents more soluble carbon fraction with lower aromaticity than C1–C3. C5 with low emission wavelength of 260/332 nm was attributable to protein-like materials containing tyrosine and tryptophan (Bilal et al., 2010), which is often observed in DBC derived from lignin-rich feedstocks (Uchimiya et al., 2013; Li et al., 2017).

The component distributions of DBCs are presented in Fig. 3f. The sums of C1 and C2 indicating humic-like substances varied differently in DBCs as a function of HTTs. It is observed that humic-like substances in DBCs derived from LIG-rich biochar (i.e. PS, BS and LIG biochar) were increased from 34.51% to 47.19%, 26.58% to 72.99% and 33.45% to 37.84%, respectively with the increase of HTTs from 300 to 500 °C. On the contrary, the humic-like substances in DBCs derived from CEL-rich biochar (i.e. CS, CC and CEL biochar) were either declined or slightly increased from 63.96% to 54.52%, 54.37% to 57.44% and 49.08% to 40.55% respectively. C4 (microbial degradation products of humics) were increased in most DBCs as a function of HTT except those from BS, PS and CEL biochar. It is observed that C4 reached over 46% for DCC500 and DLIG500. In addition, significant differences in the C4 (fulvic-like substance) between the DBCs derived from LIG-rich biochar (0–8.43%) and those from CEL-rich biochar (24.09–33.07%) was shown under the HTT of 300 °C, while they were all increased in the investigated DBCs upon the rise of HTT and reached more than 40% for DPS500, DCS500, DCC500 and DCEL500. Reversely, distinctively high C5 ranging from 42.18% to 70.08% among DPS300, DBS300 and DLIG300 but quite low with less than 21.52% among DCS300, DCC300 and CEL300 were illustrated, however, they were all significantly declined with the increase of HTTs. In summary, the fluorescence components of DBCs were closely related to the biopolymer compositions and HTTs. The humic- and protein-like substances were mainly contained in DBCs derived from LIG-rich biochar, however the humic- and fulvic-like substances were predominant in those from CEL-rich biochar at the HTT of 300 °C. The increase of HTT resulted in general decrease of protein-like substances

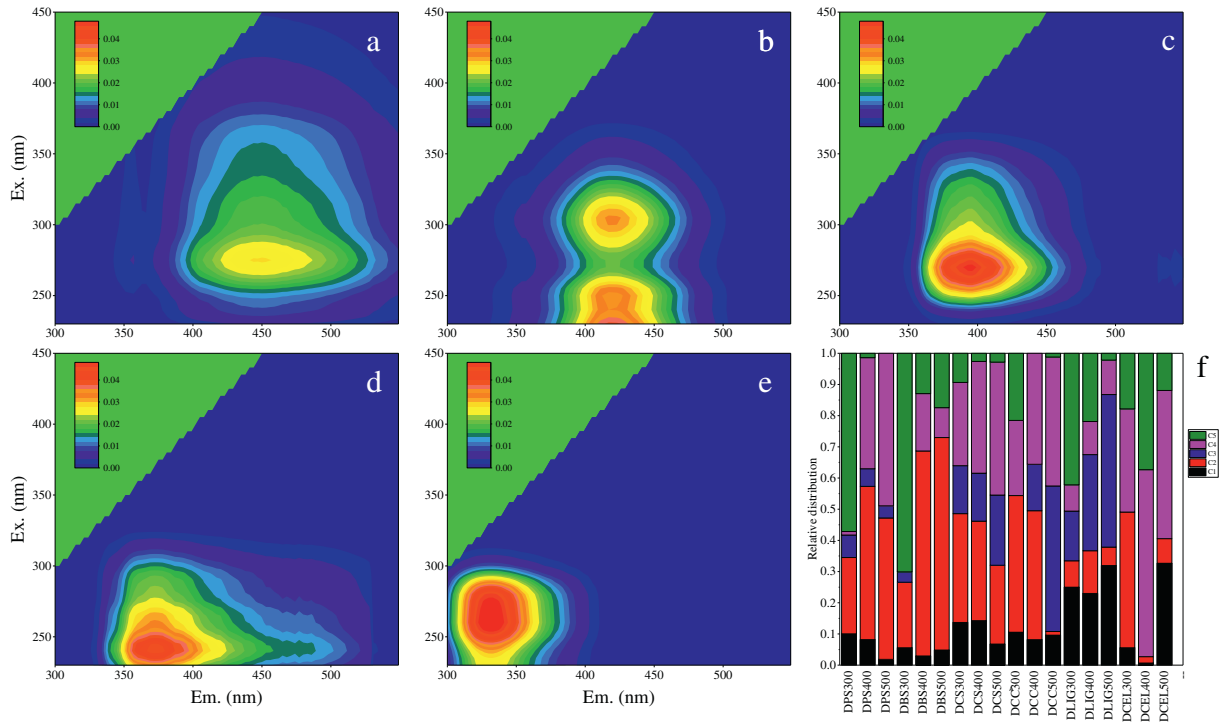

Fig. 3. Contour plots of five EEM-PARAFAC components: (a) C1, (b) C2, (c) C3, (d) C4, (e) C5; (f) their relative distribution in dissolved black carbons. Note: C1, C2 and C3 represent humic-like components; C4 and C5 represent fulvic-like and protein-like components, respectively; all values are given from five replicates; the number followed by the abbreviated letters in (f) represents the heat treatment temperatures.

and relative increase of fulvic-like substances in most DBCs, however, general increase and reduction of humic-like substances were individually observed in DBCs derived from LIG- and CEL-rich biochar. Thus, combining with the HIX values, it became obvious that the humification of DBCs derived from LIG-rich biochar was stronger than those from CEL-rich biochar under the HTT of 400 °C and 500 °C.

3.4. FTIR analysis

FTIR spectra analysis is utilized to highlight the differences in surface chemical functional groups between DBCs derived from LIG- and CEL-rich biochar (Fig. 4). Locations of main absorbance peaks for DBCs were consistent with the published data (Qu et al., 2016; Song et al., 2019). Combining our previous FTIR analysis of bulk CEL, HEM and LIG biochar (Han et al., 2016), it is noted that DBCs encompassed more abundant functional groups relative to the bulk biochar, consistent with other reported results (Song et al., 2019). On the basis of unified concentrations, Fig. 4a indicated significant differences in functional groups among DCEL300, DHEM300 and DLIG300. It is identified that DLIG300 was mainly characterized by aromatic skeletal mode (C═C and C—H) at 1600 and 900–700 cm^{-1} peaks, C═O stretching in amides at 1650 cm^{-1} peaks, aliphatic -CH_2 at 1440 cm^{-1} peaks, pyranose ring skeletal mode (C-O-C) at 1140 cm^{-1} peak, oxhydryl association (C-OH) at 1110 and 1044 cm^{-1} peak. In comparison with DLIG300, more aromatic ketone and carbonyl (C═O and COOH) functional groups at 1700 cm^{-1} peak, and ether C—O at 1222 cm^{-1}, but less aromatic and pyranose ring skeletal modes were contained in DCEL300 and DHEM300. Moreover, the FTIR spectra of DCS300, DCC300, DPS300 and DBS300 contained similar functional groups with different intensities of absorbance peaks. This is supported by stronger signals of aromatic C═O, COOH and aliphatic -CH_2 in DCC300 and aromatic C═C, C—H and C-OH stretching in DCS300, but weaker signals of pyranose ring skeletal mode (C-O-C) in both DCC300 and DCS300 than those in DBCs from LIG-rich biochar (DPS300 and DBS300), implying the functional groups of DBC being associated with the portions of biopolymer compositions. Compared to DLIG300, remarkable absorption peaks were shown at 1454, 1380, 1113 and 900–700 cm^{-1} related to aliphatic -CH_2, aliphatic –OH and phenolic –OH, and aromatic C—H species for DLIG500 indicating the weakening aromaticity, which was consistent with the increase of E_2/E_3 ratio of 9.96 for DLIG500. In addition, only moderate signals at 1710 and 1590 cm^{-1} associated with aromatic C═C and aromatic C═O, COOH were illustrated for DCEL500. Accordingly, the absorption peaks of DCS500, DCC500, DPS500 and DBS500 were close to those of DLIG500. Moreover, the characteristic absorption peaks of DLIG500 were also predominantly identified in micro particle biochar (< 1 μm) derived from wood chip, barley grass, wheat straw and peanut shell (Liu et al., 2019). Therefore, great differences in the characterized functional groups between DBCs derived from LIG and CEL (HEM) biochar were illustrated. The combined effects of three components on the surface functional groups of DBCs were marketable under the HTT of 300 °C, while that of LIG was notably pronounced following the rise of HTT.

3.5. Zeta potential and particle size analysis

To further evaluate the heterogeneities in surface charges and size variations, zeta potential and mean particle diameters of the DBCs under HTT of 300 °C were measured. The zeta potential and mean D_h of DBCs exhibited a continuous decline with pH increasing from 1.50 to 6.00 (Fig. 5a-b). The deprotonation of the ionizable functional groups, such as carboxylic and phenolic groups formed more surface negative charges at higher pH values, leading to high electronic double layer potential on the surface of DBC molecules and strong molecular repulsion (Song et al., 2019; Pan et al., 2008), which is favorable for DBCs keeping stable in aqueous solution. It is noted that the surface electronegativity of DLIG300, DPS300 and DBS300 characterized by zeta potentials ranging from 0.20 to −18.00 mV, were slightly higher than those of DCEL300, DHEM300, DCS300 and DCC300 (0.18 to −11.1 mV). This observation suggests that the DBCs from LIG-rich biochar were considered to be more stable and mobile than those from CLE-rich biochar, which

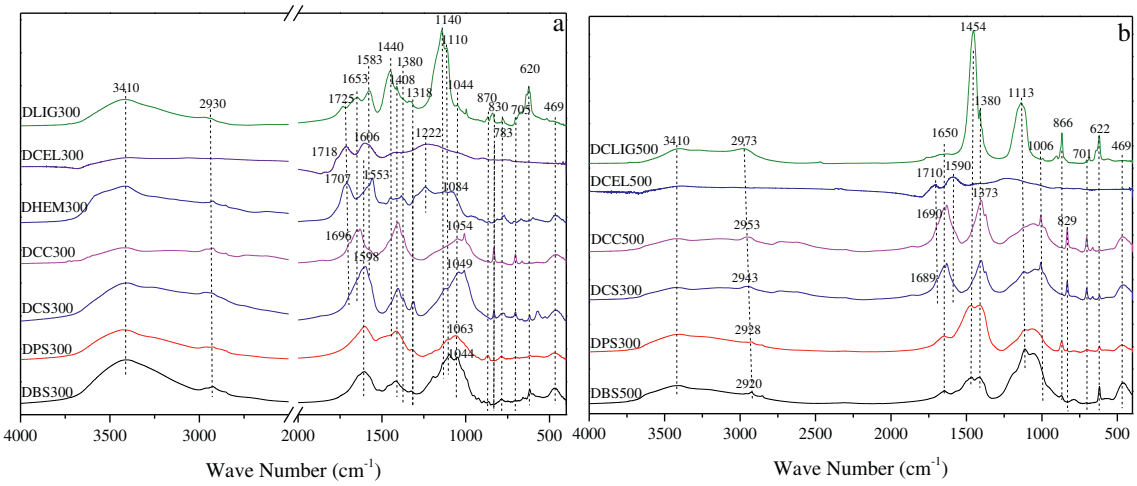

Fig. 4. FTIR spectra of dissolved black carbons derived from biochar under the HTT of 300 °C (a) and 500 °C (b). The number followed by the abbreviated letters represents HTT. Note: DBS, DCC, DCS, DPS, DCEL, DHEM and DLIG represents DBCs derived from bamboo sawdust, corncob, corn straw, pinewood sawdust lignin, cellulose and hemicellulose biochar, respectively. The number followed the abbreviated letters represents the heat treatment temperature.

was also supported by the differences in the D_h of DBCs. It is identified that lower mean molecular D_h of 326.8, 560.8, and 608.2 nm for DLIG300, DBS300 and DPS300 respectively than those of DCEL300, DHEM300, DCS300 and DCC300 (631.5, 673.4, 619.8 and 643.2 nm) under circum-neutral pH conditions (Fig. 5c-d and Fig. S5). This observation suggests that DBCs derived from LIG-rich biochar could facilitate the mobility relative to those from CEL-rich biochar. Therefore, the proportion of LIG in lignocellulosic biomass, to a certain extent, affected the migration of DBC in the environment.

4. Conclusion

Based on the analysis of physicochemical characteristics of DBCs derived from three biopolymer compositions (CEL, HEM, LIG) and four

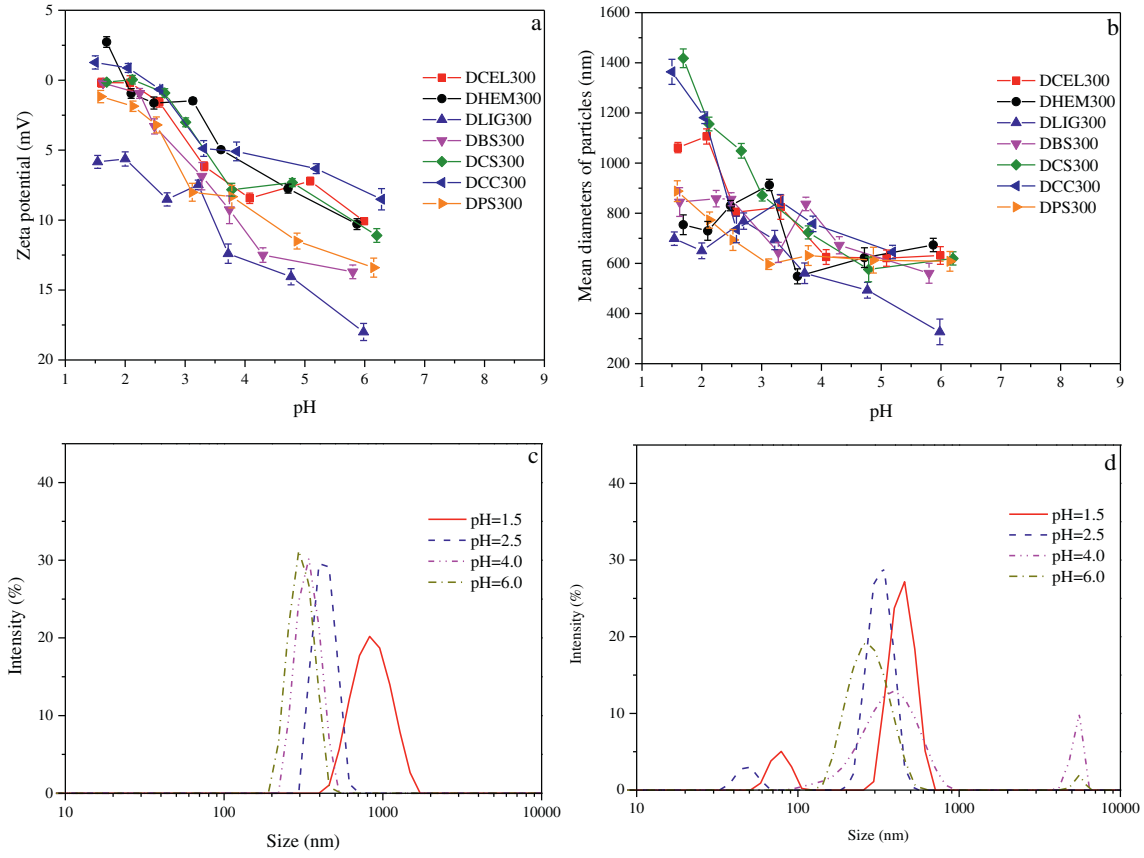

Fig. 5. (a) Zeta potential, (b) mean diameter of DBC derived from different biochar, (c) and (d) size distribution of DHEM300 and DLIG300 under different pH. Note: the DOC concentration of DBCs was 10 mg/L. DBS, DCC, DCS, DPS, DCEL, DHEM and DLIG represents DBCs derived from bamboo sawdust, corncob, corn straw, pinewood sawdust lignin, cellulose and hemicellulose biochar, respectively; the number followed the abbreviated letters represents the heat treatment temperature.

lignocellulosic biomasses (CS, CC, BS, PS) under different HTTs (i.e. 300, 400, 500 °C), it is concluded that large variations in physiochemical properties of DBC derived from CEL, HEM and LIG biochar existed under various HTTs. The obtained DBCs derived from the given lignocellulosic biomasses were most likely to be composed during the pyrolysis of CEL and HEM under HTTs of 300 and 400 °C, while LIG may be the main contributor to the DBC formation under higher HTTs (>500 °C) due to the decomposition or carbonization of CEL and HEM in the pyrolysis. Generally, CEL and HEM compositions may facilitate the release of DBCs from bulk biochar. However, on the rise of HTTs, abundant graphitic structures were formed in biochar, which was unfavorable for the release of DBCs. Reflecting the characteristics of three biopolymer compositions under the low HTT of 300–400 °C, DBCs contained abundant surface functional groups and relative high aromaticity and M_w, which were declined or diminished and close to those of LIG under the high HTT of 500 °C. Five fluorescent components were identified based on the EEM-PARAFAC analyses. Moreover, the distribution of the PARAFAC components were closely related to the biopolymer compositions and the increase of HTT resulted in general decrease of protein-like substances and relative increase of fulvic-like substances in most DBCs. LIG in biomass may facilitate the migration of DBCs due to abundant surface negative charges and the formation of low D_h. This study offered new insights into our understanding of the influencing mechanisms of biopolymer compositions on the characteristic of DBCs under different HTTs.

Declaration of competing interest

The authors declare that they have no known competing financial interests or personal relationships that could have appeared to influence the work reported in this paper.

Acknowledgments

This article is financially supported by the National Key Research and Development Program (NO. 2017YFA0207003 and 2017YFA0207002) of the Ministry of Sciences and Technology of China, the National Natural Science Foundation of China (NO. 41907170), the General Program (NO. 41471404 and 41501522) and International Cooperation and Exchanges (NO. 41761134091) of National Natural Science Foundation of China.

Appendix A. Supplementary data

Supplementary data to this article can be found online at https://doi.org/10.1016/j.scitotenv.2020.141491.

References

Aiken, G.R., Hsu-Kim, H., Ryan, J.N., 2011. Influence of dissolved organic matter on the environmental fate of metals, nanoparticles, and colloids. Environ. Sci. Technol. 45, 3196–3201.

Ando, H., Sakaki, T.S., Kokusho, T., Shibata, M., Uemura, Y., Hatate, Y., 2000. Decomposition behavior of plant biomass in hot-compressed water. Ind. Eng. Chem. Res. 39 (10), 3688–3693.

Bilal, M., Jaffrezic, A., Dudal, Y., Le, G.C., Menasseri, S., Walter, C., 2010. Discrimina-tion of farm waste contamination by fluorescence spectroscopy coupled with multivariate analysis during a biodegradation study. J. Agric. Food Chem. 58, 3093–3100.

Biswas, B., Singh, R., Kumar, J., Singh, R., Gupta, P., Krishna, B.B., Bhaskar, T., 2018. Pyrolysis behavior of rice straw under carbon dioxide for production of bio-oil. Renew. Energy 129, 686–694.

Cao, L.C., Yua, I.K.M., Liu, Y.Y., Ruan, X.X., Tsang, D.C.W., Hunt, A.J., Ok, Y.S., Song, H., Zhang, S.C., 2018. Lignin valorization for the production of renewable chemicals: state-of-the-art review and future prospects. Bioresour. Technol. 269, 465–475.

Chen, J., Gu, B.H., LeBoeuf, E.J., Pan, H.J., Dai, S., 2002. Spectroscopic characterization of the structural and functional properties of natural organic matter fractions. Chemosphere 48 (1), 59–68.

Chen, M., Wang, D., Yang, F., Xu, X., Xu, N., Cao, X., 2017. Transport and retention of biochar nanoparticles in a paddy soil under environmentally-relevant solution chemistry conditions. Environ. Pollut. 230, 540–549.

Chen, M., Alim, N., Zhang, Y., Xu, N., Cao, X., 2018. Contrasting effects of biochar nanoparticles on the retention and transport of phosphorus in acidic and alkaline soils. Environ. Pollut. 239, 562–570.

Chen, W., Habibul, N., Liu, X.Y., Sheng, G.P., Yu, H.Q., 2015. FTIR and synchronous fluorescence heterospectral two-dimensional correlation analyses on the binding characteristics of copper onto dissolved organic matter. Environ. Sci. Technol. 49, 2052–2058.

Deenik, J.L., McClellan, T., Uehara, G., Antal, M.J., Campbell, S., 2010. Charcoal volatilematter content influences plant growth and soil nitrogen transformations. Soil Sci. Soc. Am. J. 74, 1259–1270.

Fan, L., Zhang, Y., Liu, S., Zhou, N., Chen, P., Cheng, Y., Addy, M., Lu, Q., Omar, M.M., Liu, Y., Wang, Y., Dai, L., Anderson, E., Peng, P., Lei, H., Ruan, R., 2017. Bio-oil from fast pyrolysis of lignin: effects of process and upgrading parameters. Bioresour. Technol. 241, 1118–1126.

Fellman, J.B., Hood, E., Spencer, R.G.M., 2010. Fluorescence spectroscopy opens new windows into dissolved organic matter dynamics in freshwater ecosystems: a review. Limnol. Oceanogr. 55, 2452–2462.

Gai, C., Dong, Y., Zhang, T., 2013. The kinetic analysis of the pyrolysis of agricultural residue under non-isothermal conditions. Bioresour. Technol. 127, 298–305.

Han, L., Qian, L.B., Yan, J.C., Chen, M., 2016. Contributions of different biomass components to the sorption of 1,2,4-trichlorobenzene under a series of pyrolytic temperatures. Chemosphere 156, 262–271.

Han, L., Qian, L.B., Yan, J.C., Chen, M., 2017. Effects of the biochar aromaticity and molecular structures of the chlorinated organic compounds on the adsorption characteristics. Environ. Sci. Pollut. Res. 24, 5554–5565.

He, Q., Ding, L., Gong, Y., Li, W.F., Wei, J.T., Yu, G.S., 2019. Effect of torrefaction on pinewood pyrolysis kinetics and thermal behavior using thermogravimetric analysis. Bioresour. Technol. 280, 104–111.

He, W., Lee, J.H., Hur, J., 2016. Anthropogenic signature of sediment organic matter probed by UV-visible and fluorescence spectroscopy and the association with heavy metal enrichment. Chemosphere 150, 184–193.

Huang, M., Li, Z., Luo, N., Yang, R., Wen, J., Huang, B., Zeng, G., 2019. Application potential of biochar in environment: insight from degradation of biochar-derived DOM and complexation of DOM with heavy metals. Sci. Total Environ. 646, 220–228.

Ishii, S.K.L., Boyer, T.H., 2012. Behavior of reoccurring PARAFAC components in fluorescent dissolved organic matter in natural and engineered systems: a critical review. Environ. Sci. Technol. 46, 2006–2017.

Jamieson, T., Sager, E., Gueguen, C., 2014. Characterization of biochar-derived dissolved organic matter using UV-visible absorption and excitation-emission fluorescence spectroscopies. Chemosphere 103, 197–204.

Kellerman, A.M., Kothawala, D.N., Dittmar, T., Tranvik, L.J., 2015. Persistence of dissolved organic matter in lakes related to its molecular characteristics. Nat. Geosci. 8, 454–459.

Kercher, A.K., Nagle, D.C., 2003. Microstructural evolution during charcoal carbonization by X-ray diffraction analysis. Carbon 41, 15–27.

Kim, H.B., Kim, S.H., Jeon, E.K., Kim, D.H., Tsang, D.C.W., Alessi, D.S., Kwon, E.E., Baek, K., 2018. Effect of dissolved organic carbon from sludge, rice straw and spent coffee ground biochar on the mobility of arsenic in soil. Sci. Total Environ. 636, 1241–1248.

Lee, M.H., Ok, Y.S., Hur, J., 2018. Dynamic variations in dissolved organic matter and the precursors of disinfection by-products leached from biochars: leaching experiments simulating intermittent rain events. Environ. Pollut. 242, 1912–1920.

Li, J.F., Li, Y.M., Wu, Y.L., Zheng, M.Y., 2014. A comparison of biochars from lignin, cellulose and wood as the sorbent to an aromatic pollutant. J. Hazard. Mater. 280, 450–457.

Li, M., Zhang, A.F., Wu, H.M., Liu, H., Lv, J.L., 2017. Predicting potential release of dissolved organic matter from biochars derived from agricultural residues using fluorescence and ultraviolet absorbance. J. Hazard. Mater. 334, 86–92.

Lian, F., Xing, B.S., 2017. Black carbon (biochar) in water/soil environments: molecular structure, sorption, stability, and potential risk. Environ. Sci. Technol. 51, 13517–13532.

Lin, Y., Munroe, P., Joseph, S., Henderson, R., Ziolkowski, A., 2012. Water extractable organic carbon in untreated and chemical treated biochars. Chemosphere 87 (2), 151–157.

Liu, G.C., Zheng, H., Jiang, Z.X., Zhao, J., Wang, Z.Y., Pan, B., Xing, B.S., 2018. Formation and physicochemical characteristics of nano biochar: insight into chemical and colloidal stability. Environ. Sci. Technol. 52, 10369–10379.

Liu, H.C., Chun, W.Y., Li, H., Boyd, S.A., Teppen, B.J., Mao, J.D., Lehmann, J., Zhang, W., 2019. Quantification and characterization of dissolved organic carbon from biochars. Geoderma 335, 161–169.

Liu, W.J., Jiang, H., Yu, H.Q., 2015. Development of biochar-based functional materials: toward a sustainable platform carbon material. Chem. Rev. 115 (22), 12251–12285.

Norwood, M.J., Louchouarn, P., Kuo, L.J., Harvey, O.R., 2013. Characterization and biodegradation of water-soluble biomarkers and organic carbon extracted from low temperature chars. Org. Geochem. 56, 111–119.

Ouyang, D., Yan, J.C., Qian, L.B., Chen, Y., Han, L., Su, A.Q., Zhang, W.Y., Ni, H., Chen, M., 2017. Degradation of 1,4-dioxane by biochar supported nano magnetite particles activating persulfate. Chemosphere 184, 609–617.

Pan, B., Ghosh, S., Xing, B.S., 2008. Dissolved organic matter conformation and its interaction with pyrene as affected by water chemistry and concentration. Environ. Sci. Technol. 42, 1594–1599.

Qian, L.B., Zhang, W.Y., Yan, J.C., Han, L., Gao, W.G., Liu, R.Q., Chen, M., 2016. Effective removal of heavy metal by biochar colloids under different pyrolysis temperatures. Bioresour. Technol. 206, 217–224.

Qu, X.L., Fu, H.Y., Mao, J.D., Ran, Y., Zhang, D.N., Zhu, D.Q., 2016. Chemical and structural properties of dissolved black carbon released from biochars. Carbon 96, 759–767.

Schmidt, M.W.I., Torn, M.S., Abiven, S., Dittmar, T., Guggenberger, G., Janssens, I.A., Kleber, M., Kogel-Knabner, I., Lehmann, J., Manning, D.A.C., Nannipieri, P., Rasse, D.P., Weiner,

S., Trumbore, S.E., 2011. Persistence of soil organic matter as an ecosystem property. Nature 478, 49–56.
Shao, X.Y., Wang, J., Liu, Z.T., Hu, N., Liu, M., Xu, Y.W., 2020. Preparation and characterization of porous microcrystalline cellulose from corncob. Ind. Crop. Prod. 151 (1), 112457.
Smith, C.R., Sleighter, R.L., Hatcher, P.G., Lee, J.W., 2013. Molecular characterization of inhibiting biochar water-extractable substances using electrospray ionization fourier transform ion cyclotron resonance mass spectrometry. Environ. Sci. Technol. 47 (23), 13294–13302.
Soja, G., Wimmer, B., Rosner, F., Faber, F., Dersch, G., von Chamier, J., et al., 2018. Compost and biochar interactions with copper immobilisation in copper-enriched vineyard soils. Appl. Geochem. 88, 40–48.
Song, B.Q., Chen, M., Zhao, L., Qiu, H., Cao, X.D., 2019. Physicochemical property and colloidal stability of micron- and nanoparticle biochar derived from a variety of feedstock sources. Sci. Total Environ. 661, 685–695.
Tao, W.M., Duan, W.Y., Liu, C.B., Zhu, D.D., Si, X.X., Zhu, R.Z., Oleszczuk, P., Pan, B., 2020. Formation of persistent free radicals in biochar derived from rice straw based on a detailed analysis of pyrolysis kinetics. Sci. Total Environ. 715, 136575.
Tripathi, M., Sahu, J.N., Ganesan, P., 2016. Effect of process parameters on production of biochar from biomass waste through pyrolysis: a review. Renew. Sust. Energ. Rev. 55, 467–481.
Uchimiya, M., Ohno, T., He, Z.Q., 2013. Pyrolysis temperature-dependent release of dissolved organic carbon from plant, manure, and biorefinery wastes. J. Anal. Appl. Pyrolysis 104, 84–94.
Wang, Y., Hu, Y., Zhao, X., Wang, S., Xing, G., 2013. Comparisons of biochar properties from wood material and crop residues at different temperatures and residence times. Energy Fuel 27, 5890–5899.
Wang, Y., Zhang, W., Shang, J.Y., Shen, C.Y., Joseph, S.D., 2019. Chemical aging changed aggregation kinetics and transport of biochar colloids. Environ. Sci. Technol. 53, 8136–8146.
Wei, J., Tu, C., Yuan, G.D., Bi, D.X., Wang, H.L., Zhang, L.J., Theng, B.K.G., 2019. Pyrolysis temperature-dependent changes in the characteristics of biochar-borne dissolved organic matter and its copper binding properties. Bull. Environ. Contam. Toxicol. 103, 169–174.
Yang, H.P., Yan, R., Chen, H., Lee, D.H., Zheng, C., 2007. Characteristics of hemicellulose, cellulose and lignin pyrolysis. Fuel 86 (12−13), 1781–1788.
Yang, L., Choi, J.H., Hur, J., 2014. Benthic flux of dissolved organic matter from lake sediment at different redox conditions and the possible effects of biogeochemical processes. Water Res. 61, 97–107.
Yang, R., Xu, S., Wang, Z., Yang, W., 2005. Aqueous extraction of corncob xylan and production of xylooligosaccharides. LWT 38, 677–682.
Yang, X., Tsibart, A., Nam, H., JinHur, J., Naggar, A.E., Tack, F.M.G., Wang, C.H., Lee, Y.H., Tsang, D.C.W., Ok, Y.S., 2019. Effect of gasification biochar application on soil quality: trace metal behavior, microbial community and soil dissolved organic matter. J. Hazard. Mater. 365, 684–694.
Zhao, L., Zheng, W., Cao, X., 2014. Distribution and evolution of organic matter phases during biochar formation and their importance in carbon loss and pore structure. Chem. Eng. J. 250, 240–247.
Zhao, Y., Feng, D., Zhang, Y., Huang, Y., Sun, S., 2016. Effect of pyrolysis temperature on char structure and chemical speciation of alkali and alkaline earth metallic species in biochar. Fuel Process. Technol. 141, 54–60.
Zhong, D.L., Zhao, Z.Z., Jiang, Y., Yang, X., Wang, L.L., Chen, J., Guan, C.Y., Zhang, Y.R., Tsang, D.C.W., Crittenden, J.C., 2020. Contrasting abiotic As(III) immobilization by undissolved and dissolved fractions of biochar in Ca^{2+} rich groundwater under anoxic conditions. Water Res., 116106
Zhong, W.Z., Zhang, Z.Z., Luo, Y.J., Sun, S.S., Qiao, W., Xiao, M., 2011. Effect of biological pretreatments in enhancing corn straw biogas production. Bioresour. Technol. 102 (24), 11177–11182.